J. Fluid Mech. (1987), *vol.* 180, *pp.* 297–318
Printed in Great Britain

Waves due to a steadily moving source on a floating ice plate. Part 2

By R. M. S. M. SCHULKES, R. J. HOSKING AND A. D. SNEYD
University of Waikato, Hamilton, New Zealand

(Received 10 April 1986 and in revised form 26 November 1986)

This paper extends previous theoretical work on waves in floating ice plates to take account of the following effects: (i) compressive stress in the plane of the plate, (ii) uniform flow in the underlying water, and (iii) stratification of the underlying water. The first two effects are unlikely to be important in practice, causing respectively a slight decrease in phase speed and mainly a re-orientation of the wave pattern due to a steadily moving source. A two-layer model is used to describe stratification, which introduces a new system of slow internal waves associated with the layer interface, while the surface flexural waves are only slightly modified. In the case of unstratified water there is a minimum speed $c_{\min}$ such that more slowly moving sources excite a static rather than a wavelike response in the ice. With stratified water there remains a variety of steady wave patterns due to the internal waves, at source speeds below $c_{\min}$. Another important effect of stratification is to greatly increase wave drag. For certain source load distributions, internal-wave amplitudes may grow until linear theory is no longer applicable.

1. Introduction

An earlier paper (Davys, Hosking & Sneyd 1985, hereafter referred to as Paper I), discussed flexural wave patterns excited in a floating ice plate by a steadily moving load. It was shown that the pattern of these elastic–gravity waves depends on the speed of the source, and that the response amplitude, frequency and phase depend on the thickness and elastic properties of the ice. The mathematical model assumed an elastic homogeneous ice plate of infinite extent resting on incompressible inviscid fluid of constant depth.

In this sequel paper we discuss a number of effects referred to but not studied in Paper I. Section 2 deals with a lateral stress imposed on the ice plate, and although we conclude that this is unimportant in practice the modified dispersion relation does have features of theoretical interest. In §3 we note that a uniform sea current under the ice also modifies the dispersion relation and hence the wave pattern, but the effects may be difficult to detect. Of greater significance is stratification in the underlying water which we discuss in §4 using a two-layer model. The internal-wave propagation that then occurs is an interesting classical matter of potential practical importance, especially as regards the energy of the wave system (cf. Lamb 1945; Garrett & Munk 1979).

2. Compressive stress on the ice

Thermal strain, surface friction due to a prevailing wind, and water flow beneath the ice are three natural sources of compressive stress in a floating ice plate, and the

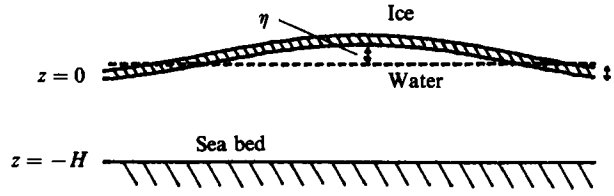

FIGURE 1. Diagram of floating ice plate.

effects of such stress on wave propagation have been considered by Kerr (1979, 1983) and Bates & Shapiro (1980). We consider the same model used by these authors – an infinite homogeneous ice plate of thickness h and density ρ_i under lateral stress and resting on water of uniform depth H (see figure 1). We use a Cartesian coordinate system with (x, y) in the undisturbed lower plane surface of the ice plate $z = 0$, as in Paper I. The small vertical deflection of the ice plate is denoted by $\eta(x, y, t)$, and including the lateral stress term $T\nabla^2\eta$ (compressive for $T > 0$), we adopt the modified equation of motion:

$$D\nabla^4\eta + T\nabla^2\eta + \rho_i h\eta_{tt} = p - f(x, y, t), \tag{2.1}$$

where $D = Eh^3/[12(1-\nu^2)]$ is the modulus of rigidity which depends sensitively on ice thickness h (as well as Young's modulus E and Poisson's ratio ν), p is the water pressure at $z = 0$, $f(x, y, t)$ is the downward external stress exerted on the ice by the moving source, and $\nabla^2 = \partial^2/\partial x^2 + \partial^2/\partial y^2$ is the planar Laplacian operator. Assuming that the underlying water is incompressible and its flow is irrotational with velocity potential $\phi(x, y, z, t)$, from Bernoulli's theorem we have

$$p = -\rho(\phi_t)_{z=0} - \rho g\eta, \tag{2.2}$$

so (2.1) becomes

$$D\nabla^4\eta + T\nabla^2\eta + \rho_i h\eta_{tt} = -\rho(\phi_t)_{z=0} - \rho g\eta - f. \tag{2.3}$$

Unless otherwise stated, throughout this paper we adopt the parameter values of Paper I (for the ice at McMurdo Sound, Antarctica) – viz. $E = 5 \times 10^9$ N m^{-2}, $h = 2.5$ m, $H = 350$ m, and $\nu = \frac{1}{3}$. The densities of ice and sea water may be taken to be $\rho_i = 917$ kg m^{-3} and $\rho = 1024$ kg m^{-3}, and the gravitational acceleration $g = 9.81$ m s^{-2}. We shall find that the lateral stress T has to be very large to produce measurable effects on the wave propagation.

2.1. *Dispersion relation*

The dispersion relation for uniform plane waves, with η everywhere proportional to $\exp[\mathrm{i}(\boldsymbol{k}\cdot\boldsymbol{x} - \omega t)]$, follows from (2.3) and the kinematic (non-cavitation) boundary condition

$$\eta_t = (\phi_z)_{z=0} = k \tanh(kH)\,(\phi)_{z=0};$$

thus setting $f = 0$ we get

$$\omega^2 = \frac{Dk^5/\rho - Tk^3/\rho + gk}{kh' + \coth kH}, \quad h' = \frac{\rho_i h}{\rho}. \tag{2.4a}$$

As discussed in Paper I, there are three important lengthscales associated with the dispersion relation – a short scale, characterized by the (modified) ice thickness h'; a long scale, characterized by the water depth H; and an intermediate scale $k_{\min}^{-1}$ characterized by the reciprocal of the wavenumber $k_{\min}$ at which the phase speed $c = \omega/k$ is a minimum, depending on the ice elasticity and gravity, and also the stress

T in this context. At short wavelengths ($kh' \geqslant O(1)$) we have elastic-dominated waves appearing ahead of the source, and at long wavelengths ($kH \leqslant O(1)$) gravity waves behind the source, but the imposed stress might modify the important intermediate wavelengths.

Provided the wavelength is large compared with ice thickness ($kh' \ll 1$), we may neglect the ice acceleration term in the denominator of (2.4*a*) and use

$$\omega^2 = \left[\frac{Dk^4 - Tk^2}{\rho g} + 1\right] gk \tanh kH, \tag{2.4b}$$

as an approximate dispersion relation. The physical basis of this approximation is that the wave motion penetrates the water to a depth of order one wavelength, so the inertia of this moving water layer will be much larger than the inertia of the relatively thin ice plate. For waves of intermediate length such that $k_{\min} h' \ll 1$ and $k_{\min} H \gg 1$ (typically $k_{\min}^{-1} \approx 50$ m), the phase speed is

$$c = \left[\frac{Dk^3 - Tk}{\rho} + \frac{g}{k}\right]^{\frac{1}{2}}, \tag{2.5}$$

so increasing the compressive stress T slows the wave. We recall that lowering the tension, or increasing lateral compression, reduces the speed of propagation of waves in a stretched string or membrane. The minimum phase speed (identified in Paper I, equation (2.5)) is moderated by the stress: i.e.

$$c_{\min} = 2\left(\frac{Dg^3}{27\rho}\right)^{\frac{1}{8}} e^{-\epsilon/4} [\tfrac{1}{2}(3 - e^{2\epsilon})]^{\frac{1}{4}}, \quad \epsilon = \sinh^{-1}\left(\frac{T}{(12\rho g D)^{\frac{1}{2}}}\right).$$

This minimum phase speed is zero for $T = 2(\rho g D)^{\frac{1}{2}} = T_c$ say, when $k_{\min} = (\rho g/D)^{\frac{1}{4}}$. We deduce from (2.4*b*) that for stability ($\omega^2 > 0$) the compressive stress may not exceed T_c, which Kerr (1983) associated with buckling of an elastic plate. This situation is somewhat different from the classical buckling problem in that buckling is resisted not only by the elastic rigidity of the plate, but also by the underlying water which provides a further restoring force independent of wavelength.

The group speed $c_g = \mathrm{d}\omega/\mathrm{d}k$ for intermediate wavelengths ($k_{\min} h' \ll 1$, $k_{\min} H \gg 1$) can be written

$$c_g = \frac{1}{2\omega}\left[\frac{5D}{\rho}\left(k^2 - \frac{3T}{10D}\right)^2 + g - \frac{9T^2}{20\rho D}\right], \tag{2.6}$$

which (for $\omega > 0$) is positive definite for $T < \frac{1}{3}(20\rho g D)^{\frac{1}{2}} = T_{cg}$ say. In theory the group speed can be zero or even negative when ($T_{cg} \leqslant T \leqslant T_c$). Such stress values however are much higher than anticipated in the field (see below), so a stationary observer is unlikely to see the curious spectacle of wave crests moving in one direction, whilst the wave group remains stationary or even moves in the opposite direction. The phase and group speeds are plotted against wavenumber in figure 2(*a*, *b*), with the representative parameters already mentioned, for zero stress and for the critical values T_{cg} and T_c. Note that when $T = T_c$ and c has a zero at k_0 say, one can write

$$c = k^{-\frac{1}{2}} |k^2 - k_0^2|,$$

so the graph of c against k has a cusp at k_0, and the graph of c_g a discontinuity at that same point. For small compressive stresses there is a nearly linear decrease with respect to T, according to

$$c_{\min} \approx 2\left(\frac{Dg^3}{27\rho}\right)^{\frac{1}{8}} (1 - \tfrac{3}{4}\epsilon), \quad \epsilon \ll 1.$$

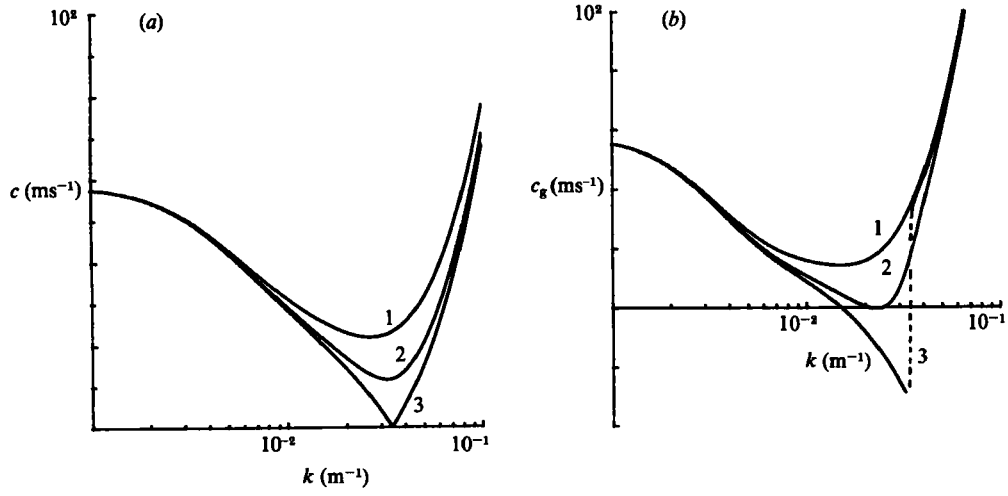

FIGURE 2. Variation of phase speed c and group speed c_g with wavenumber k for different values of the lateral stress T: curve 1, $T = 0$; curve 2, $T = T_{cg}$; curve 3, $T = T_{cr}$. Note that the wavenumber scale is logarithmic.

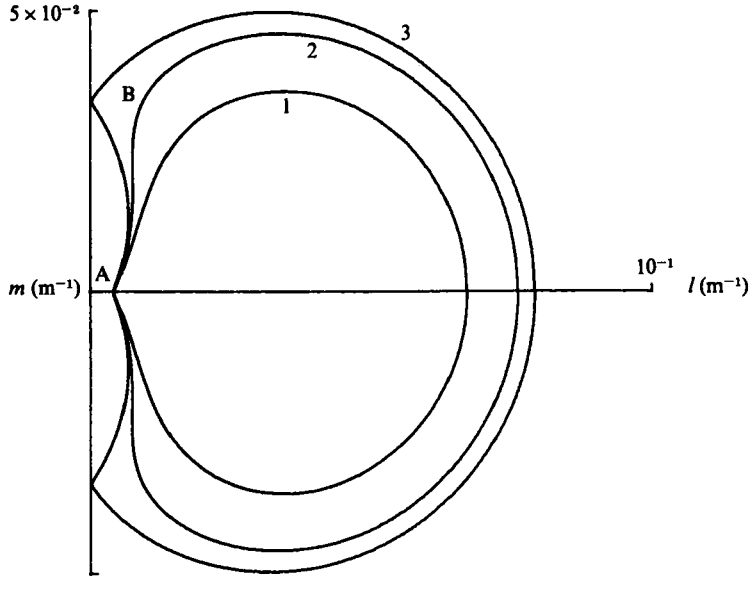

FIGURE 3. Wavenumber curves at supercritical source speed $V = 45$ m s^{-1}, for various values of the lateral stress T: curve 1, $T = 0$; curve 2, $T = T_{cg}$; curve 3, $T = T_{cr}$.

Seifert & Langleben (1972) estimate that a 5–10 m s^{-1} wind over 100 km of ice may produce a lateral compressive stress in the range 3×10^3–3×10^4 N m^{-1}, which corresponds to $\epsilon \leqslant 100 D^{-\frac{1}{2}}$ so that $\epsilon \ll 1$ unless the ice is only centimeters thick. It would be surprising if thermal strain or water flow beneath the ice were to generate stresses of comparable magnitude.

2.2. *Wavenumber curve and the wave pattern*

For a steady wave pattern relative to the source, at each point on a wave crest the phase speed must equal the component of the source velocity normal to the crest – i.e.

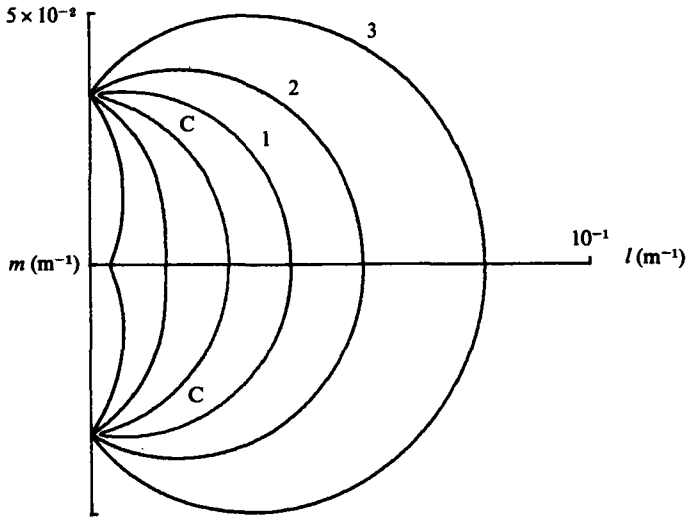

FIGURE 4. Wavenumber curves at critical lateral stress ($T = T_{cr}$) for various source speeds: curve 1, $V = 6$ m s^{-1}; curve 2, $V = 20$ m s^{-1}; curve 3, $V = 45$ m s^{-1}. Note that the curves tend towards the circular arc $k = (\rho g/D)^{\frac{1}{4}}$ as $V \to 0$.

$c = V\cos\beta$, where β is the angle between the direction of the wavenumber vector $\boldsymbol{k} = (l, m)$ and the source velocity $\boldsymbol{V}$. Orienting the axes so that the source moves in the positive x-direction, the equation of the wavenumber curve corresponding to dispersion relation (2.4) is

$$Dk^4 - Tk^2 + \rho g - \rho h' V^2 l^2 - \frac{\rho V^2 l^2}{k} \coth kH = 0. \tag{2.7}$$

Waves propagate in directions normal to the wavenumber curve. Features of the curve geometry, which depend on the source speed, produce an interesting variety of wave patterns (cf. Paper I).

The possible variation of the wavenumber curve due to a lateral stress is shown in figure 3, where at supercritical source speed ($V = 45$ m s$^{-1} > c_{min}$) the wavenumber curves at the rather high critical stresses T_{cg} and T_c may be compared with the unstressed case $T = 0$. An increase in the compressive stress results in a larger wavenumber curve (conversely, we found that a tensile stress reduces its size), and we note that the gravity-wave region becomes vertical when $T = T_{cg}$, and the curve bends back towards the m-axis for $T_{cg} < T < T_c$. The wavenumber curve does shrink to a point as $V \to c_{min}$ (cf. Paper I), for $T < T_c$. The curious theoretical behaviour shown in figure 4 corresponds to an earlier observation that for $T = T_c$, $c_{min} = 0$ when $k = (\rho g/D)^{\frac{1}{4}}$, which is the radius of the circular arc towards which the wavenumber curves tend in the limit $V \to 0$. The wave patterns corresponding to the curves of figure 3 are shown in figure 5 (a–c). In figure 5 (a) the corresponding wavenumber curve (curve 1 in figure 3) has two points of inflexion on each side of the l-axis, so each crest in the gravity-wave region has four cusps (cf. figure 6c in Paper I). In figure 5 (b) the inner cusps now lie on the x-axis, since the corresponding point of inflexion occurs where the wavenumber curve (curve 2 in figure 3) is vertical. In figure 5 (c) the inner cusps have moved to the opposite side of the x-axis since the outward normal at the point of inflexion A on the wavenumber curve (curve 3 in figure 3) has a positive m-component, and that at B a negative m-component. When $T = T_{cr}$ the wavenumber curve tends to a circular arc centred at the origin as $V \to 0$, and the wave crests tend

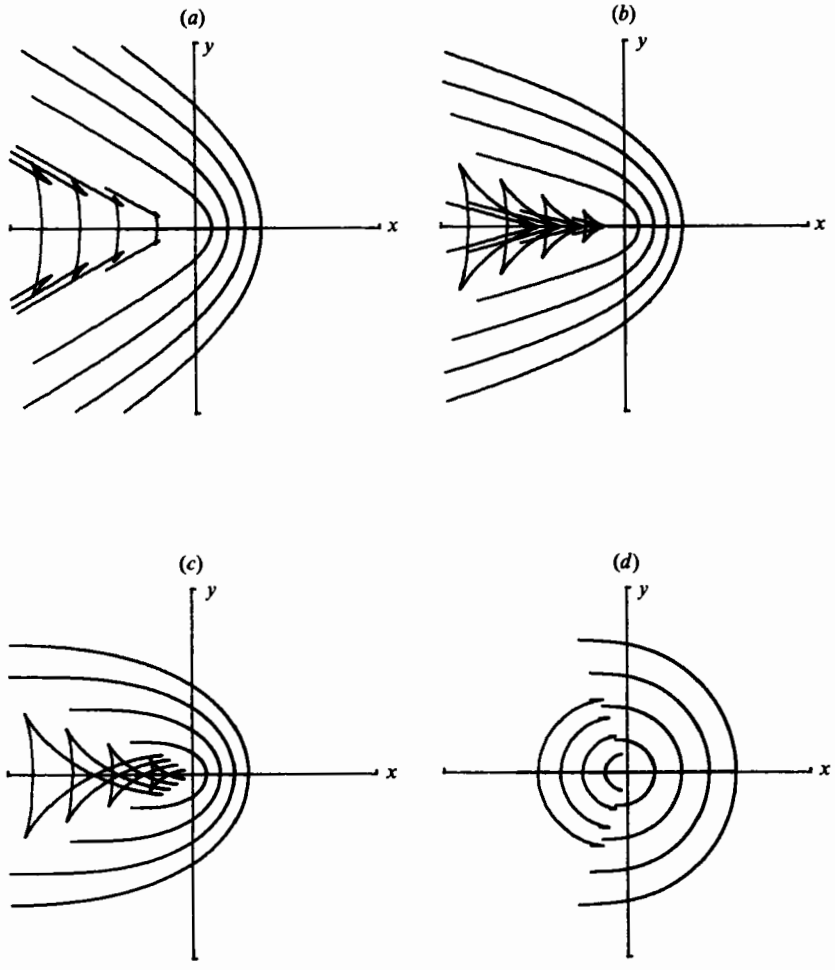

FIGURE 5. Wave patterns for $V = 45$ m s^{-1} and (*a*) $T = 0$, (*b*) $T = T_{cg}$, (*c*) $T = T_{cr}$ respectively. (*d*) Wave pattern for $V = 6$ m s^{-1} and $T = T_{cr}$.

to concentric circles. Figure 5(*d*) shows a wave crest pattern (for a small value of V) which differs only slightly from this limiting form. Cusps have appeared corresponding to the point of inflexion C on curve 1 in figure 4.

3. Flow underneath the ice

Let us now ignore lateral stress in the ice, but suppose that the water beneath the ice flows uniformly with constant velocity $\boldsymbol{U} = (U_x, U_y, 0)$, so $\boldsymbol{U}+\boldsymbol{\nabla}\phi$ is the perturbed velocity during wave motion. The linearized Bernoulli equation for the pressure at $z = 0$,

$$p = -\rho(\phi_t + \boldsymbol{U}\cdot\boldsymbol{\nabla}\phi)_{z=0} - \rho g\eta,$$

replaces (2.2), so the modified dynamic equation of the ice plate becomes

$$D\nabla^4\eta + \rho_i h\eta_{tt} + \rho g\eta = -\rho(\phi_t + \boldsymbol{U}\cdot\boldsymbol{\nabla}\phi)_{z=0} - f. \tag{3.1}$$

3.1. *Dispersion relation*

Including the relative flow, the kinematic (non-cavitation) boundary condition is

$$\eta_t + \boldsymbol{U}\cdot\nabla\eta = (\phi_z)_{z=0} = k\tanh kH\,(\phi)_{z=0},$$

hence the dispersion relation obtained from (3.1) is

$$\frac{Dk^5}{\rho} + gk - kh'\omega^2 - (\omega - \boldsymbol{k}\cdot\boldsymbol{U})^2\coth kH = 0. \tag{3.2}$$

For the same reason as in §2, we neglect the ice acceleration term $kh'\omega^2$ to obtain

$$\omega_{\mathrm{D}}^2 = \left(\frac{Dk^4}{\rho g} + 1\right) gk\tanh kH, \tag{3.3}$$

where $\omega_{\mathrm{D}} = \omega - \boldsymbol{k}\cdot\boldsymbol{U}$ is the Doppler-shifted frequency relative to an observer moving with the water. Note that (3.3) is identical with the dispersion relation for still water (equation (2.6) in Paper I), except that ω_{D} replaces ω. This is to be expected since transforming to a frame of reference moving with the water is equivalent to imposing a translational velocity $-\boldsymbol{U}$ on the ice plate. This does not affect the elastic restoring term $D\nabla^4\eta$ in (3.1) which is calculated by static methods, under the assumption that flexural waves are much slower than any purely elastic waves.

The ice acceleration term in (3.1) is affected, involving a material derivative, but it is of course neglected in (3.3). We therefore expect the flow to otherwise influence slightly the dispersion at very short wavelengths ($kh' \geqslant O(1)$), when the relevant approximation to (3.2) is

$$\omega_{\mathrm{D}}^2 = \frac{Dk^4}{\rho h'} - \boldsymbol{k}\cdot\boldsymbol{U}\left[k^2\left(\frac{D}{\rho h'}\right)^{\frac{1}{2}} + \boldsymbol{k}\cdot\boldsymbol{U}\right]. \tag{3.4}$$

3.2. *Wavenumber curve and the wave pattern*

In a frame of reference moving with the water, the transformed source velocity is $\boldsymbol{V}_r = \boldsymbol{V} - \boldsymbol{U}$. Choosing the x-axis in this frame to be parallel to $\boldsymbol{V}_r$, the equation of the wavenumber curve based on (3.2) is

$$\frac{Dk^4}{\rho} + gk - kh'[l(U_x + V_r) + mU_y]^2 - (lV_r)^2\coth kH = 0, \tag{3.5}$$

where now $-\boldsymbol{U}$ is to be interpreted as the transverse velocity of the ice plate. On setting $m = -m$, we observe that the wavenumber curve is no longer quite symmetric about the l-axis – an effect of the anisotropy mentioned above.

As shown in figure 6, for an observer moving with the flow, there is only a slight alteration of the wavenumber curve at short wavelengths even for a rather large relative value of the transverse velocity. To an observer on the ice, however, the wave pattern will no longer be aligned with the source velocity but rotated through an angle

$$\delta = \tan^{-1}\left(\frac{U_y}{V - U_x}\right), \tag{3.6}$$

as shown in figure 7. Even for the very largest tidal currents (or order 1 m s^{-1}) it may be that neither effect would be easy to detect.

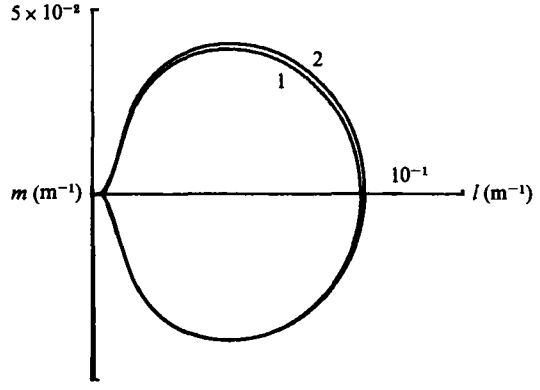

FIGURE 6. Slight anisotropy of the wavenumber curve due to a uniform flow under the ice, perpendicular to the source velocity. For curve 1, $U_y = 0$; curve 2, $U_y = 10$ m s^{-1}; and in each case the source velocity $V = 50$ m s^{-1}.

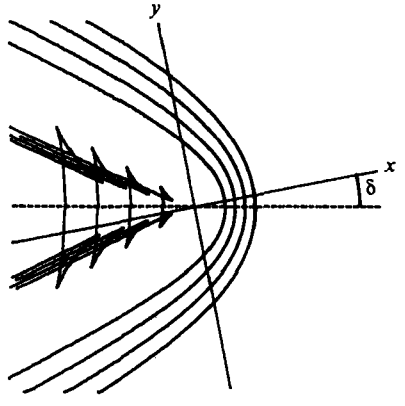

FIGURE 7. Influence on the wave-crest pattern of a uniform flow under the ice normal to the source velocity. The pattern is now almost symmetric about the direction of $V-U$ – the velocity of the source relative to the water – which is indicated by a dashed line.

4. Water stratification

In this section we neglect any imposed stress or sea currents, but suppose that the underlying water is stratified. Stratification may be caused by freezing or melting of the ice, and exhibits rather complicated seasonal variations (see e.g. Lewis & Walker 1970). For simplicity we adopt a two-layer model – a layer of density ρ_1 resting above a layer of density ρ_2. In the undisturbed state we denote the interface of the two layers by $z = -H_1$ and the total depth to the bottom of the second layer by $z = -H_2$, as shown in figure 8. This is similar to the model used by Lamb (1935, article 231) to describe fresh water from the land overlying sea water in estuaries or fiords.

We again let $\eta(x, y, t)$ represent the small deflection of the ice plate and introduce $\xi(x, y, t)$ to represent the small displacement of the internal interface between the two layers. We assume both layers are incompressible, with their irrotational motion described by the two velocity potentials $\phi_1(x, y, z, t)$ and $\phi_2(x, y, z, t)$ respectively, which are related by the continuity of pressure condition (via Bernoulli equations)

$$\rho_1(\phi_{1t} + g\xi)_{z=-H_1} = \rho_2(\phi_{2t} + g\xi)_{z=-H_1}, \tag{4.1}$$

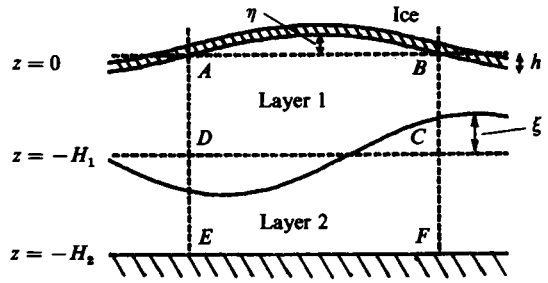

FIGURE 8. Diagram of ice plate floating above two water layers.

and the kinematic conditions

$$\xi_t = (\phi_{1z})_{z=-H_1} = (\phi_{2z})_{z=-H_1}. \tag{4.2}$$

The dynamic equation of the ice plate is of course

$$D\nabla^4\eta + \rho_i h\eta_{tt} + \rho_1 g\eta = -\rho_1(\phi_{1t})_{z=0} - f. \tag{4.3}$$

The kinematic conditions at the ice–water surface and at the rigid bottom are

$$\eta_t = (\phi_{1z})_{z=0}, \quad (\phi_{2z})_{z=-H_2} = 0. \tag{4.4a,b}$$

4.1. *Dispersion relation*

Assuming sinusoidal waves $\eta = \eta_0 \exp[\mathrm{i}(\boldsymbol{k}\cdot\boldsymbol{x} - \omega t)]$ and $\xi = \xi_0 \exp[\mathrm{i}(\boldsymbol{k}\cdot\boldsymbol{x} - \omega t)]$, we find the velocity potentials satisfying (4.4) must be of the form:

$$\phi_1 = (A\cosh kz - \mathrm{i}\omega\eta_0 k^{-1}\sinh kz)\exp[\mathrm{i}(\boldsymbol{k}\cdot\boldsymbol{x} - \omega t)], \tag{4.5}$$

$$\phi_2 = B\cosh[k(z+H_2)]\exp[\mathrm{i}(\boldsymbol{k}\cdot\boldsymbol{x} - \omega t)], \tag{4.6}$$

where the constants A, B and the internal amplitude ξ_0 satisfy a system of three equations obtained from (4.1) and (4.2): in matrix form

$$\begin{bmatrix} \rho_1\cosh kH_1 & -\rho_2\cosh k(H_2-H_1) & g(\rho_2-\rho_1)/\mathrm{i}\omega \\ \sinh kH_1 & \sinh k(H_2-H_1) & 0 \\ 0 & \sinh k(H_2-H_1) & \mathrm{i}\omega/k \end{bmatrix} \begin{bmatrix} A \\ B \\ \xi_0 \end{bmatrix} = \begin{bmatrix} -(\mathrm{i}\omega/k)\rho_1\eta_0\sinh kH_1 \\ -(\mathrm{i}\omega/k)\eta_0\cosh kH_1 \\ 0 \end{bmatrix}.$$

Solving this system of equations, we find in particular that

$$\phi_1 = -\frac{\mathrm{i}\omega}{k}(\mu\cosh kz + \sinh kz)\eta, \tag{4.7}$$

where we conveniently define

$$\mu = \coth kH_1 \frac{\rho_1\tanh kH_1 + \rho_2\coth k(H_2-H_1) - gk(\rho_2-\rho_1)/\omega^2}{\rho_1\coth kH_1 + \rho_2\coth k(H_2-H_1) - gk(\rho_2-\rho_1)/\omega^2}; \tag{4.8}$$

and the ratio of the displacement amplitude at the ice–water surface to the amplitude at the internal interface is

$$\frac{\xi_0}{\eta_0} = \frac{\rho_1}{\sinh kH_1[\rho_1\coth kH_1 + \rho_2\coth k(H_2-H_1) - gk(\rho_2-\rho_1)/\omega^2]}. \tag{4.9}$$

Note that since ξ_0/η_0 is real and positive, the surface and interfacial waves are in phase.

The dispersion relation for uniform plane waves follows from (4.7) and the equation of motion (4.3) with $f = 0$; we have

$$\omega^2 = \frac{Dk^5/\rho_1 + gk}{kh' + \mu}, \quad h' = \frac{\rho_1 h}{\rho_1}. \tag{4.10}$$

The expression designated by μ (cf. (4.8)) contains ω^2 terms, so dispersion relation (4.10) is a quadratic in ω^2. Solving for ω^2, we obtain the explicit quadratic roots

$$\omega_{\pm}^2 = \frac{Q \pm (Q^2 - 4PR)^{\frac{1}{2}}}{2P}, \tag{4.11}$$

where writing $\lambda = 1 + Dk^4/(\rho_1 g)$ we have

$$P = \rho_1 + \rho_2 \coth kH \coth k(H_2 - H_1) + kh' [\rho_1 \coth kH_1 + \rho_2 \coth k(H_2 - H_1)], \tag{4.12a}$$

$$Q = gk[(\rho_2 - \rho_1) \coth kH_1 + \lambda(\rho_1 \coth kH_1 + \rho_2 \coth k(H_2 - H_1)) + kh'(\rho_2 - \rho_1)], \tag{4.12b}$$

$$R = g^2 k^2 (\rho_2 - \rho_1) \lambda. \tag{4.12c}$$

The two explicit quadratic roots (4.11) might have been expected since the system has virtually two degrees of freedom, involving both surface flexural (elastic–gravity) waves at $z = 0$ and internal waves at $z = -H_1$ (cf. Lamb 1945).

In passing, we note that earlier results are limiting cases of dispersion relation (4.10):

(i) When $\rho_1 \to \rho_2$ or $H_1 \to H_2$ we have $\mu \to \coth kH_2$, and recover the classical dispersion relation for an ice plate floating on a uniform fluid of density ρ_1 (Greenhill 1887). With reference to (4.12) we note that $R \to 0$ when $\rho_1 \to \rho_2$, so the two quadratic roots (4.11) reduce to $\omega^2 = Q/P$ and $\omega^2 = 0$; and we note that the term in R is also negligible when $H_1 \to H_2$.

(ii) In the limit $H_1 \to 0$ we get

$$\mu \to \frac{\rho_2 \coth kH_2 - gk(\rho_2 - \rho_1)/\omega^2}{\rho_1},$$

and from (4.10) recover the classical dispersion relation for an ice plate floating on a uniform fluid of density ρ_2.

(iii) From (4.12) we also note that the limit $h \to 0$ (and hence $D \to 0$) yields the dispersion relations for waves at the free surface and at the internal interface of the two fluid layers, when there is no ice plate (cf. Lamb 1945).

4.2. *Approximate expressions for the dispersion relation*

For the various characteristic wavelength regimes described earlier, we now obtain useful approximate expressions for the two quadratic roots (4.11) of the dispersion relation. Once again there are three important lengthscales: the short lengthscale h'; an important intermediate scale, $k_{\min}^{-1}$; and a long lengthscale, H_2 in this context. We continue to assume that the ice cover is relatively thin, so that $h' \ll H_1 < H_2$.

Short wavelengths

In the case of very short waves ($kh' > O(1)$), (4.12) become respectively

$$P = (1 + kh')(\rho_1 + \rho_2),$$

$$Q = \frac{Dk^5(\rho_1 + \rho_2)}{\rho_1},$$

$$R = \frac{gDk^6(\rho_2 - \rho_1)}{\rho_1}.$$

Since the elastic parameter D is very large (typically 10^9), the term $Q^2 \approx D^2k^{10}$ dominates the discriminant in (4.11), so we may take a first-order binomial approximation to obtain

$$\omega_{\pm}^2 \approx \frac{Q \pm Q(1-2PR/Q^2)}{2P}. \tag{4.13}$$

On substituting the short-wave approximations immediately above, we therefore have

$$\omega_+^2 \approx \frac{(1+kh')^{-1}Dk^5}{\rho_1}, \tag{4.14a}$$

$$\omega_-^2 \approx \frac{gk(\rho_2-\rho_1)}{\rho_1+\rho_2}. \tag{4.14b}$$

In the limit $kh' \gg 1$ we see that (4.14*a*) reduces to the earlier dispersion relation for flexural elastic waves in ice floating on uniform fluid of density ρ_1 (cf. Paper I). Equation (4.14*b*) describes gravitational internal waves (if $\rho_1 < \rho_2$) at the interface of the two superposed fluids of infinite extent (cf. Lamb 1945). We note that because the density difference of the two layers is typically rather small ($|\rho_2-\rho_1| \ll \rho_1, \rho_2$), the period of oscillation of the internal gravity waves can be very large compared with the period of the surface flexural waves. (In fact it emerges that the phase speed of the flexural waves ω_+/k is generally much higher than the phase speed ω_-/k of internal waves.) Finally we recall that elastic-dominated ice waves appear ahead of the source (cf. Paper I), whereas these internal gravity waves fall behind.

Intermediate wavelengths

For all but the shortest wavelengths, we again entirely neglect the kh' terms. Thus for waves of intermediate length ($k = O(k_{\min})$), suitable approximations for (4.10) are

$$P = \rho_1 + \rho_2 \coth kH_1,$$

$$Q = \rho_2\left(gk + \frac{Dk^5}{\rho_1}\right)\left[1 + \frac{gk + Dk^5/\rho_2}{gk + Dk^5/\rho_1}\coth kH_1\right],$$

$$R = \left(gk + \frac{Dk^5}{\rho_1}\right)gk(\rho_2-\rho_1).$$

It has again been assumed that the depth is large compared with the wavelength, which may however now be comparable with the depth of the upper layer, i.e. $kH_2 \gg 1$ but $kH_1 = O(1)$. The binomial approximation (4.13) is again valid, so that for intermediate wavelengths we have the respective quadratic roots for flexural and internal waves:

$$\omega_+^2 \approx \frac{Dk^5}{\rho_1}\frac{\rho_1 \coth kH_1 + \rho_2}{\rho_2 \coth kH_1 + \rho_1} + gk\frac{1+\coth kH_1}{\rho_1/\rho_2 + \coth kH_1}, \tag{4.15a}$$

$$\omega_-^2 \approx gk\left(1-\frac{\rho_1}{\rho}\right)\left[1 + \frac{gk + Dk^5/\rho_2}{gk + Dk^5/\rho_1}\coth kH_1\right]^{-1}. \tag{4.15b}$$

Equations (4.15) reduce to (4.14) if we set $kH_1 = \infty$, and neglect the gravity term gk in the case of (4.15*a*). The stronger elastic–gravity hybrid character of the flexural

waves is again evident. If the density difference is small ($|\rho_2-\rho_1| \ll \rho_1, \rho_2$), (4.15) reduce to

$$\omega_+^2 \approx \frac{Dk^5}{\rho_1}+gk,$$

$$\omega_-^2 \approx gk\left(1-\frac{\rho_1}{\rho_2}\right)[1+\coth kH_1]^{-1}.$$

The earlier remark concerning the oscillation period or relative phase speed of the flexural and internal waves is again relevant.

Long wavelengths

For long wavelengths, comparable with the total depth ($kH_2 < O(1)$), the approximations for (4.10) are

$$P = \rho_1+\rho_2 \coth kH_1 \coth k(H_2-H_1),$$

$$Q = gk\rho_2[\coth kH_1+\coth k(H_2-H_1)],$$

$$R = g^2k^2(\rho_2-\rho_1).$$

Once again, the binomial approximation (4.11) is appropriate, so we obtain

$$\omega_+^2 \approx gk\rho_2\left[\frac{\coth kH_1+\coth k(H_2-H_1)}{\rho_1+\rho_2 \coth kH_1 \coth k(H_2-H_1)}\right], \tag{4.16a}$$

$$\omega_-^2 \approx gk\left(1-\frac{\rho_1}{\rho_2}\right)[\coth kH_1+\coth k(H_2-H_1)]^{-1}. \tag{4.16b}$$

Thus for long wavelengths both the flexural and internal waves are gravity-dominated, and depend on the depth of both the upper and lower layers. If we set $kH_2 = \infty$ in (4.16), we recover the approximations (4.15), on neglecting the elastic term. When $H_1 \ll H_2$, (4.16*a*) reduces to the well-known dispersion for gravity waves on water of depth H_2, i.e. $\omega_+^2 = gk \tanh kH_2$.

4.3. *Phase and group speeds*

In figure 9, the phase and group speed are plotted against wavenumber, for the flexural (ω_+) and internal (ω_-) waves respectively. We assume that the upper layer is salt water of density $\rho_1 = 1024$ kg m^{-3}, and the lower layer salt water of density $\rho_2 = 1025.3$ kg m^{-3}, to model the water column beneath fast ice. A typical upper-layer thickness of order $H_1 = 10$ m should be representative, and we take the total depth $H_2 = 350$ m as before. Note that the phase and group speeds of the internal waves are significantly less than those of the flexural wave at all wavelengths, attain their maximum in the long-wavelength limit, and decrease gradually as the wavelength decreases (i.e. as k increases). In the long-wavelength limit ($k \to 0$), from (4.16*b*) we find that the common value of the phase and group speeds of the internal wave is $[g(1-\rho_1/\rho_2)(H_2-H_1)H_1/H_2]^{\frac{1}{2}}$. Differentiating this expression with respect to H_1, we conclude that the phase and group speeds of the internal wave are maximum in this long-wavelength limit when $H_1 = \frac{1}{2}H_2$, and this case is also represented in figure 9(*b*). The phase and group speeds of the flexural wave represented in figure 9(*a*) are insensitive to stratification (cf. figure 2 of Paper I).

4.4. *Amplitude ratios*

We may further assess the importance of internal waves, with respect to the response of the ice–water system at supercritical source speeds ($V > c_{\min}$), by considering the relative amplitude of internal to flexural waves defined by (4.9).

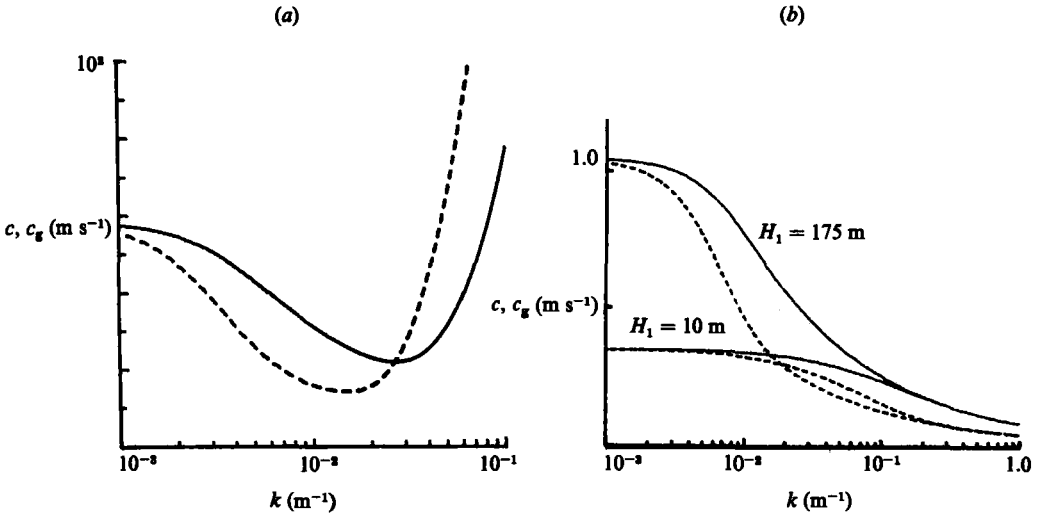

FIGURE 9. (*a*) Graphs of phase speed c (——) and group speed c_g (– – –) against wavenumber k for flexural waves with stratified water. These are insensitive to water depth H_1. (*b*) Corresponding graphs for the internal-wave branch. Note that the wavenumber scale is logarithmic.

Let us first consider the ω_+ (flexural-wave) case, for which it is convenient to use the approximations obtained in the last section. In the short-wavelength limit, we invoke (4.14*a*) to get

$$\frac{\xi_0}{\eta_0} = \frac{2\rho_1 \, \mathrm{e}^{-kH_1}}{\rho_1+\rho_2}. \tag{4.17a}$$

For waves of intermediate length, we use (4.15*a*) to find

$$\frac{\xi_0}{\eta_0} = \frac{\rho_1}{\rho_1 \cosh kH_1 + \rho_2 \sinh kH_1}, \tag{4.17b}$$

and from (4.16*a*) for wavelengths we have

$$\frac{\xi_0}{\eta_0} = \frac{\rho_1}{\sinh kH_1[\rho_1 \coth kH_1 + \rho_2 \coth k(H_2-H_1)]}. \tag{4.17c}$$

Obviously, (4.17) are self-consistent, in that (4.17*c*) reduces to (4.17*b*) which reduces to (4.17*a*), as the wavelength decreases (i.e. as k increases). If the upper layer is shallow ($H_1 \ll H_2$) we have $\xi_0/\eta_0 \to 1$ in the long-wavelength limit, cf. (4.17*c*). This is as anticipated, since surface waves typically penetrate to a depth of the order of one wavelength. The short-wavelength limit is dominated by the exponential factor, so that $\xi_0/\eta_0 \to 0$, i.e. the disturbance is strongly localized at the ice–water surface.

The amplitude ratio in the ω_- (internal-wave) case can be expressed (cf. Appendix A):

$$\frac{\xi_0}{\eta_0} = -\frac{1+Dk^4/(\rho_1 g)}{\rho_2-\rho_1}[\rho_1 \coth kH_1 + \rho_2 \coth k(H_2-H_1)] \sinh kH_1 + \cosh kH_1 + kh' \sinh kH_1. \tag{4.18}$$

In the limit $k \to 0$ we have $\xi_0/\eta_1 \to 1-\rho_1/(\rho_2-\rho_1)$, so when the density difference is small even the longer-wavelength internal waves will not penetrate to the ice–water surface.

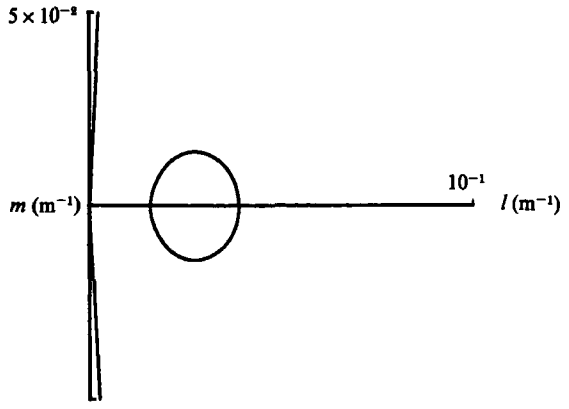

FIGURE 10. Representative wavenumber curve for stratified water at supercritical speed ($V > c_{\min}$). The flexural wave (roughly circular) branch is largely unaffected by the stratification (cf. figure 4, Paper I). The section of the internal-wave branch shown is approximately straight on each side of the l-axis. (As $k \to \infty$ the internal branch becomes parallel to the m-axis.)

(We also have $\xi_0/\eta_0 \to -\infty$ in the short-wavelength limit, i.e. the surface response is negligible in this case too, and the disturbance is strongly localized at the interface between the water layers.)

4.5. *Wavenumber curve and wave patterns*

The condition for a steady wave pattern is as before ($c = V\cos\beta$), but now there can be two distinct branches of the wavenumber curve since there are two characteristic frequencies (ω_+ and ω_-). The two branches are shown in figure 10, for source speed $V = 25$ m s^{-1}. In the previous three subsections we noted that the surface dispersion is insensitive to stratification, so we anticipate that the corresponding branch of the wavenumber curve has the familiar approximately circular shape shown, implying that the flexural elastic–gravity waves in the ice radiate in all directions from the source (cf. Paper I). The other branch of the wavenumber curve in figure 10 (corresponding to ω_-) is not closed, at least in the absence of surface tension (cf. Longuet-Higgins 1977), so the internal waves radiate only into a narrow region behind the source. For source speeds less than the minimum phase speed of flexural waves ($c_{\min} \approx 22.5$ m s^{-1} for the physical parameters assumed), there can be no surface-wave branch of the wavenumber curve, *i.e. only the internal branch persists, so the source excites only internal waves and the flexural response is static.* For these lower speeds, the form of the internal wave pattern depends crucially on the behaviour of the wavenumber curve close to the origin, which we proceed to analyse further.

Assuming that $H_1 \ll H_2$, the equation describing the internal branch of the wavenumber curve in the long-wavelength limit (i.e. close to the origin in the (l, m)-plane) follows from (4.16*b*):

$$(V\cos\beta)^2 = gH_1\left(1-\frac{\rho_1}{\rho_2}\right)(1-\tfrac{1}{3}k^2H_1^2), \tag{4.19}$$

where we have used the small argument expansion, $\tanh kH_1 \approx kH_1(1-\frac{1}{3}k^2H_1^2)$. Defining $V_{ci}^2 = gH_1(1-\rho_1/\rho_2)$, if $V < V_{ci}$ we can re-express (4.19) as

$$k^2 = k_0^2 + \frac{3V^2}{H_1^2 V_{ci}^2}\sin^2\beta, \quad k_0 = \frac{[3(V^2 - V_{ci}^2)]^{\frac{1}{2}}}{H_1 V_{ci}}.$$

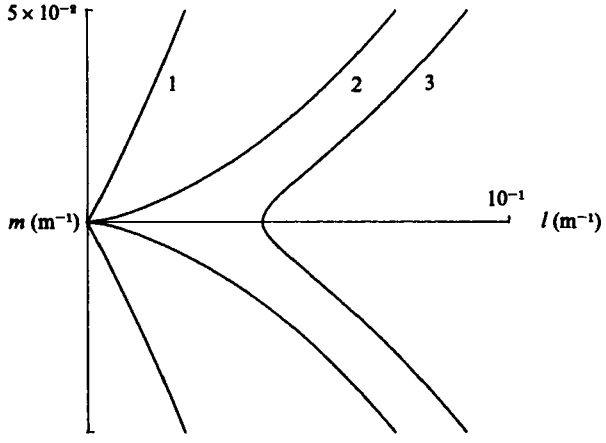

FIGURE 11. Behaviour of the internal branch of the wavenumber curve near the origin for source speeds close to V_{c1}: curve 1, $V > V_{c1}$; curve 2, $V = V_{c1}$; curve 3, $V < V_{c1}$.

Here k and β are polar coordinates, where k_0 is the point of intersection of the wavenumber curve with the l-axis when $\beta = 0$. If $V = V_{c1}$, then (4.19) becomes

$$k = \frac{\sqrt{3}\sin\beta}{H_1};$$

while for $V > V_{c1}$ we rewrite (4.19) as

$$k^2 = \frac{3V^2(\cos^2\beta - \cos^2\beta_0)}{(H_1 V_{c1})^2}, \quad \beta_0 = \cos^{-1}\left(\frac{V_{c1}}{V}\right),$$

which represents a pair of curves intersecting at the origin, each making an angle β_0 with the l-axis. This behaviour near the origin is very similar to that of the unstratified wavenumber curve when V is close to the critical speed $V_c = (gH)^{\frac{1}{2}}$ (see Paper I (3.7) and (3.8)). In this case however the critical speed is much less; $V_{c1} = [gH_1(1-\rho_1/\rho_2)]^{\frac{1}{2}} < 1$ m s^{-1} for the internal wave, compared with $V_c \approx 58.5$ m s^{-1} for the surface wave. From the short-wavelength approximation (4.14*b*) we find that for small source speed V the point of intersection of the internal-wave (ω_-) branch with the positive l-axis is given by $l = (g/V)(\rho_2-\rho_1)/(\rho_1+\rho_2)$. This point of intersection goes off to infinity as $V \to 0$. Figure 11 illustrates this behaviour by showing internal branches of wavenumber curves near the origin, for source speeds close to V_{c1}.

In figure 12(*a*) $V_{c1} < V \ll c_{min}$ and the normal directions to the corresponding wavenumber curve (cf. figure 11) all lie within the narrow range $\pi - \beta_0 \leqslant \beta \leqslant \pi + \beta_0$, so the wave pattern is confined to a triangular region behind the source. (This is very similar to the internal-gravity-wave pattern generated by steady vertical motion of a sphere through uniformly stratified fluid, shown in Lighthill 1978; figure 106.) In figure 12(*b*) $V < V_{c1}$ and the wavenumber curve is very similar to that for gravity waves on deep water (see Lighthill 1978, figure 101), so the wave pattern is rather like the Kelvin ship-wave pattern.

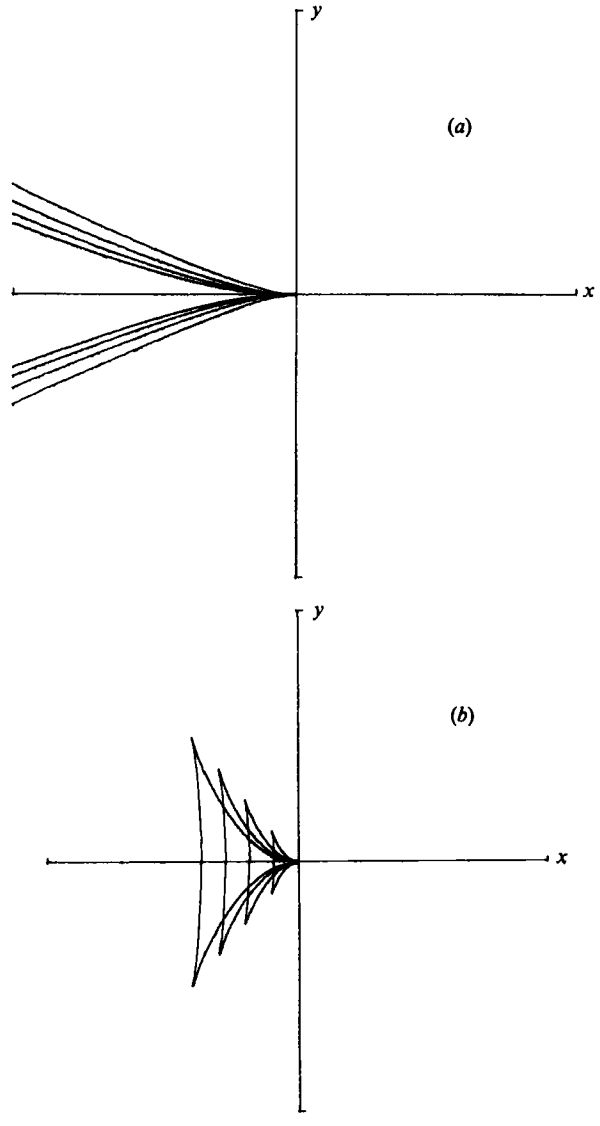

FIGURE 12. Typical internal-wave-crest patterns. In (a) $V_{ci} < V \ll c_{min}$ and the corresponding wavenumber curve has only an internal branch. In (b) $V < V_{ci}$ and the corresponding wavenumber curve (curve 3 in figure 11, for the behaviour near the origin) is similar to that for gravity waves on deep water, with one point of inflexion. Thus the wave-crest pattern is similar to the Kelvin ship-wave pattern.

4.6. *Restriction on the loading function*

A complication arises because the internal branch of the wavenumber curve is unbounded, in the absence of surface tension. From (4.14*b*) we see that when k is large, the approximate equation for C_k is

$$k = \frac{g'}{V^2 \cos^2\beta}, \quad g' = \frac{g(\rho_2 - \rho_1)}{\rho_2 + \rho_1}, \tag{4.20}$$

which is identical with the corresponding equation for gravity waves on deep water (see Lighthill 1978, figure 101).

For a steadily moving source the loading function f can be written in the form

$$f(x, y, t) = F(x - Vt, y),$$

and at large distances from the source the displacement η is given by the asymptotic formula (cf. (3.6) in Paper I):

$$\eta \approx -\hat{F}(l_0, m_0)\left(\frac{2\pi}{\kappa_0 r}\right)^{\frac{1}{2}}\left(\frac{\partial B}{\partial n}\right)^{-1} \mathrm{e}^{-\mathrm{i}(l_0 x + m_0 y + \Theta)}. \tag{4.21}$$

Here $\hat{F}$ is the Fourier transform of F and

$$B(l, m) = Dk^4 + \rho_1 g - \rho_1 h' V^2 l^2 - \rho_1 \mu V^2 l^2 / k,$$

where μ is defined by (4.8) with ω replaced by Vl. The wavenumber $\boldsymbol{k}_0 = (l_0, m_0)$ corresponds to that point P_0 on the wavenumber curve C_k which radiates waves in the direction considered, κ_0 is the curvature of C_k at P_0, and $\partial B/\partial n$ is the derivative of B at P_0 in the direction normal to C_k. If there is more than one point P_0 on the wavenumber curve which radiates waves in the given direction, then the surface displacement is the sum of contributions of the form (4.21).

Using the limiting form (4.20) of the internal-wavenumber curve, we find that the contributions to η for large k have amplitude

$$\eta_0 = -\frac{\pi^{\frac{1}{2}}}{D}\left(\frac{g(\rho_2 - \rho_1)}{(\rho_2 + \rho_1) V^2}\right)^{\frac{1}{4}} r^{-\frac{1}{2}} k^{-\frac{11}{4}}. \tag{4.22}$$

The ratio of internal to surface wave amplitude ξ_0/η_0, is given by (4.18), and is $O(k^4 \mathrm{e}^{kH_1})$ as $k \to \infty$, so it follows from (4.22) that

$$\xi_0 = O[\hat{F}(l_0, m_0)\, k^{\frac{11}{4}} \mathrm{e}^{kH_1}] \quad \text{as } k \to \infty. \tag{4.23}$$

This exponential growth for large k can be counteracted in (4.23) only by a corresponding exponential decay in $\hat{F}(l, m)$, i.e. ξ_0 will remain finite only if

$$\hat{F} = o(k^{-\frac{11}{4}} \mathrm{e}^{-kH_1}) \quad \text{as } k \to \infty. \tag{4.24}$$

If the loading function is such that (4.24) is not satisfied then our analysis breaks down, since the internal-wave amplitudes ξ_0 required for the steady wave pattern become infinitely large as $k \to \infty$, and the small-amplitude assumption would be violated. In practice, if a moving load not satisfying (4.24) were applied, the internal-wave amplitudes would grow with time from the instant of application until further growth was prevented by nonlinear effects or damping. To ensure that (4.24) were satisfied we could choose a normal distribution loading function of the form

$$F = \frac{Mg}{\pi b^2} \mathrm{e}^{-r^2/b^2}, \quad \text{with } \hat{F} = \frac{Mg}{2\pi} \mathrm{e}^{-k^2 b^2/4},$$

where M is the mass of the load, and b a constant representing its width. Another more realistic choice of loading function, based on approximating the aircraft wing by a uniform line vortex and its image in the plane $z = 0$ (see Davys 1984), is

$$F(x, y) = \frac{Mgb}{2\pi(b^2 + r^2)^{\frac{3}{2}}}, \quad \text{with } \hat{F} = \frac{Mg}{2\pi} \mathrm{e}^{-kb}, \tag{4.25}$$

where the constant b measures the lateral extent of the load, and is of order the aircraft height. The loading function (4.23) will yield finite ξ_0 provided $b > H_1$ (cf. (4.24)).

5. Wave drag on a moving source

It is well known that an important component of the drag on a ship is associated with the power loss in exciting surface or other waves. On entering an estuary in which the water is stratified, a ship may experience a substantial drag even if no surface waves are evident, due to the excitation of internal waves (e.g. Lamb 1945). In this section we consider the wave drag on a load moving over an ice plate, when the underlying water is stratified.

The mean energy density W of a plane wave (averaged over one wavelength) is the sum of the mean potential energy W_{P} and mean kinetic energy W_{K}. The elastic potential energy of the bent ice plate is $\frac{1}{4}Dk^4|\eta|^2$ (see Landau & Lifshitz 1959, p. 45) and the gravitational potential energy associated with the upper water surface $\frac{1}{4}\rho_1 g|\eta|^2$ (see Lighthill 1978, p. 212). (The absolute value signs are used on the usual understanding that η is a complex quantity proportional to $\mathrm{e}^{\mathrm{i}(kx-\omega t)}$ say, for a plane wave in the x-direction, whose real part represents the surface displacement.) Similarly the gravitational potential energy associated with the interface $z=-H_1$ is $\frac{1}{4}(\rho_2-\rho_1)g|\xi|^2$, so that the total mean potential energy is

$$W_{\mathrm{P}} = \tfrac{1}{4}(Dk^4+\rho_1 g)|\eta|^2+\tfrac{1}{4}(\rho_2-\rho_1)g|\xi|^2.$$

It is shown in Appendix B that there is equipartition of mean kinetic and potential energies, i.e. that $W_{\mathrm{K}} = W_{\mathrm{P}}$, so it follows that the total mean energy density is

$$W = \tfrac{1}{2}W_0(k)|\eta|^2, \tag{5.1}$$

where

$$W_0(k) = Dk^4+\rho_1 g+(\rho_2-\rho_1)g\left(\frac{\xi_0}{\eta_0}\right)^2. \tag{5.2}$$

Note that we have ignored the small kinetic energy of the ice plate, consistent with neglecting the ice acceleration term in the dispersion relation. For unstratified water W_0 is given by just the first two terms of (5.2).

Thus the power P required to maintain the steady wave system, or the flux of energy radiated away from the source, is given by

$$P = \int_{C_F} \tfrac{1}{2}W_0|\eta|^2(\boldsymbol{c}_{\mathrm{g}}-\boldsymbol{V})\cdot\hat{\boldsymbol{n}}\,\mathrm{d}s_F, \tag{5.3}$$

where C_F is a circle of large radius surrounding the source and moving with it, $\hat{\boldsymbol{n}}$ is the outward unit normal vector to C_F, and $\mathrm{d}s_F$ is an element of arc length along C_F. Now we can write

$$\mathrm{d}s_F = r\,\mathrm{d}\theta,$$

where (r,θ) are polar coordinates in the co-moving (x,y)-plane. The angle θ gives the direction in which waves are radiated from the source, and is equal to the angle between the normal to the wavenumber curve C_k and the l-axis, so

$$\mathrm{d}s_F = r\frac{\mathrm{d}\theta}{\mathrm{d}s}\mathrm{d}s = r\kappa\,\mathrm{d}s,$$

where s measures distance along C_k. Since the normal $\hat{\boldsymbol{n}}$ to C_k, the direction in which waves are propagated, is parallel to the relative group velocity $\boldsymbol{c}_{\mathrm{g}}-\boldsymbol{V}$, on combining (5.1), (5.3) and (4.21) we obtain

$$P = \pi\int_{C_k} W_0(k)|F(l,m)|^2\left(\frac{\partial B}{\partial n}\right)^{-2}|\boldsymbol{c}_{\mathrm{g}}-\boldsymbol{V}|\,\mathrm{d}s, \tag{5.4}$$

(cf. Lighthill 1978, equation 299).

There is an important complication – the wavefield does not always consist of single plane waves. If the wavenumber curve has the same normal direction at two separate points, then two plane waves of different wavenumber will be radiated in that direction, and the displacement η will be a superposition of these two waves. This will always occur with stratified water when C_k has two branches, for their directions must coincide over certain sections (see figure 10), and can also occur even for unstratified water, if C_k has points of inflexion (see Paper I). In any regions where two or more plane waves are present, (5.1) must be modified so that the right-hand side is some quadratic form in the various amplitudes. To avoid such complications we have carried out calculations only in the two situations where wave overlapping does not occur: (*a*) the unstratified case with $c_{\min} < V < V_s = 37.5$ m s^{-1} (see Paper I) so that no points of inflexion occur, and (*b*) the case of stratified water with $V_{ci} < V < c_{\min}$ so that only the internal branch of the wavenumber curve is present and again no points of inflexion occur.

In case (*a*) we chose a point load Mg($M = 10^4$ kg for a typical aircraft), so that

$$f = Mg\,\delta(x - Vt)\,\delta(y), \quad \hat{F} = \frac{Mg}{\pi},$$

and found that the small value of the power ($\approx 10^{-1}$ W) varied only slightly with V.

In case (*b*) the loading function $F(x, y)$ must satisfy restriction (4.24) for finite internal-wave amplitudes, if the power integral (5.4) is to converge. We chose the loading function (4.25) with $H_1 = 10$ m and found that for fixed V, as the lengthscale b tended to H_1 from above, the power increased rapidly as the integral (5.4) became more slowly convergent. Choosing a fixed value of $b = 15$ m (large enough to ensure convergence), we found a rapid increase in power as V tended to the lower limit V_{ci} from above. This corresponds to the observed behaviour of ships on stratified water in fiords, where the drag is found to reduce significantly if the speed be raised above a certain value.

6. Conclusions

Compressive stress in the plane of a floating ice plate is unlikely to have any significant effect on the propagation of waves due to a moving load. We expect only a slight reduction in the observed phase speeds, and in particular in the critical speed $c_{\min}$ which the source speed V must exceed for a dynamic rather than a static response (e.g. Squire *et al.* 1985). A flow underneath the ice re-orients the wave pattern towards symmetry about the direction of the source speed relative to the water, and introduces truly anisotropic dispersion only for wavelengths comparable with the ice thickness.

If the underlying water is stratified, a moving load excites internal waves in the water in addition to any response in the ice. For source speeds greater than $c_{\min}$ both flexural and internal waves are generated, but a slower source generates only internal waves. A very slow source may experience an anomalous drag due to these internal waves, analogous to the 'abnormal resistance' occasionally experienced by ships entering fiords in which the water is stratified (Lamb 1945). In such circumstances the drag is extremely sensitive to the loading function (whereas for unstratified water it is quite insensitive), and the internal-wave amplitudes may grow in time until limited by nonlinear effects or damping.

We are grateful to V. Squire for comment on polar conditions relevant to the calculations in this paper.

Appendix A. Amplitude ratio

The amplitude ratio (4.9) is

$$\frac{\xi_0}{\eta_0} = \frac{\rho_1}{\sinh kH_1(\rho_1 c_1+\rho_2 c_2-gk\rho_d/\omega^2)} \tag{A 1}$$

if we write $c_1 = \coth kH_1$, $c_2 = \coth k(H_2-H_1)$, and $\rho_d = \rho_2-\rho_1$. In the ω_- (internal-wave) case, the bracketed term in the denominator of (A 1) vanishes identically for $c_1 = c_2 = 1$, which is the usual approximation at short wavelength. Thus in this case we retain the exact form of the quadratic root (cf. (4.11)), so that

$$\omega_-^{-2} = \frac{Q+(Q^2-4PR)^{\frac{1}{2}}}{2R}, \tag{A 2}$$

where with $\lambda = 1+Dk^4/(\rho_1 g)$ we have

$$P = \rho_1+\rho_2 c_1 c_2+kh'(\rho_1 c_1+\rho_2 c_2),$$
$$Q = gk[\lambda(\rho_1 c_1+\rho_2 c_2)+\rho_d(c_1+kh')],$$
$$R = g^2k^2\lambda\rho_d.$$

It immediately follows that

$$\frac{Q^2-4PR}{g^2k^2} = [\lambda(\rho_1 c_1+\rho_2 c_2)-\rho_d(c_1+kh')]^2+4\lambda\rho_1\rho_d(c_1^2-1);$$

and hence

$$\left(1-\frac{4PR}{Q^2}\right)^{\frac{1}{2}} = \frac{\lambda(\rho_1 c_1+\rho_2 c_2)-\rho_d(c_1+kh')}{\lambda(\rho_1 c_1+\rho_2 c_2)+\rho_d(c_1+kh')}(1+\alpha)^{\frac{1}{2}}, \tag{A 3}$$

where

$$\alpha = \frac{4\lambda\rho_1\rho_d(c_1^2-1)}{[\lambda(\rho_1 c_1+\rho_2 c_2)-\rho_d(c_1+kh')]^2}.$$

Thus from (A 2) and (A 3) we write the bracketed term in the denominator of (A 1) as

$$\rho_1 c_1+\rho_2 c_2-gk\rho_d\omega_-^{-2} = [\lambda(\rho_1 c_1+\rho_2 c_2)-\rho_d(c_1+kh')]\frac{1-(1+\alpha)^{\frac{1}{2}}}{2\lambda}$$

$$\approx \frac{-\rho_1\rho_d(c_1^2-1)}{\lambda(\rho_1 c_1+\rho_2 c_2)-\rho_d(c_1+kh')},$$

since $|\alpha| \ll 1$ if $|\rho_d| \ll \rho_1, \rho_2$. Thus (A 1) becomes

$$\frac{\xi_0}{\eta_0} = \sinh kH_1\left[c_1+kh'-\frac{\lambda(\rho_1 c_1+\rho_2 c_2)}{\rho_d}\right]. \tag{A 4}$$

Appendix B. Proof that $W_P = W_K$

The total kinetic energy T over one wavelength is given by

$$T = \tfrac{1}{2}\rho_1 \int_{S_1} (\nabla\phi_1)^2 \,\mathrm{d}V + \tfrac{1}{2}\rho_2 \int_{S_2} (\nabla\phi_2)^2 \,\mathrm{d}V, \tag{B 1}$$

where S_1 is the interior of $ABCD$ (the upper fluid layer) and S_2 the interior of $CDEF$ (the lower fluid layer) as indicated in figure 8. We use the usual identity $(\nabla\phi)^2 = \nabla\cdot(\phi\nabla\phi)$ for harmonic functions ϕ to re-express (B 1) in terms of surface integrals:

$$T = \tfrac{1}{2}\rho_1 \int_{AB} \phi_1 \frac{\partial\phi_1}{\partial z}\,\mathrm{d}s - \tfrac{1}{2}\rho_1 \int_{CD} \phi_1 \frac{\partial\phi_1}{\partial z}\,\mathrm{d}s + \tfrac{1}{2}\rho_2 \int_{CD} \phi_2 \frac{\partial\phi_2}{\partial z}\,\mathrm{d}s, \tag{B 2}$$

where $\mathrm{d}s$ denotes an element of arc length along the boundary. Contributions from the vertical parts of the boundary cancel because of periodicity, and contributions from the bottom $z = -H_2$ vanish by virtue of (4.4b). Use of the kinematic surface conditions (4.2) and (4.4a) in (B 2) gives

$$T = \tfrac{1}{2}\rho_1 \int_{AB} \phi_1 \eta_t \,\mathrm{d}s + \frac{1}{2}\int_{CD} (\rho_2\phi_2 - \rho_1\phi_1)\,\xi_t \,\mathrm{d}s. \tag{B 3}$$

For plane waves in which the ϕ and η are both proportional to $\mathrm{e}^{\mathrm{i}(kx-\omega t)}$, (4.3) with $f = 0$ shows that on AB

$$\rho_1\phi_1 = \frac{(Dk^4 + \rho_1 g)\,\eta}{\mathrm{i}\omega}, \tag{B 4}$$

where as usual we have ignored the ice acceleration term. Since the average $\langle ab\rangle$ over one wavelength of two complex quantities a, b each proportional to $\mathrm{e}^{\mathrm{i}(kx-\omega t)}$ is $\frac{1}{2}\mathrm{Re}\,(ab^*)$, where the asterisk denotes the complex conjugate, we find using (B 4) that

$$\langle \rho_1\phi_1\eta_t\rangle = \tfrac{1}{2}(Dk^4 + \rho_1 g)\,|\eta|^2.$$

In a similar way we can use (4.1) to show that

$$\langle (\rho_2\phi_2 - \rho_1\phi_1)\,\xi_t\rangle = \tfrac{1}{2}(\rho_2 - \rho_1)\,g\,|\xi|^2,$$

so it follows that the mean kinetic energy is

$$W_K = \langle T\rangle = \tfrac{1}{4}(Dk^4 + \rho_1 g)\,|\eta|^2 + \tfrac{1}{4}(\rho_2 - \rho_1)\,|\xi|^2,$$

which is identical with the expression for the mean potential energy.

REFERENCES

Bates, H. F. & Shapiro, L. H. 1980 Long period gravity waves in ice-covered sea. *J. Geophys. Res.* **85**, 1095–1100.

Davys, J. W. 1984 Waves in floating ice plates. M.Sc. thesis, University of Waikato.

Davys, J. W., Hosking, R. J. & Sneyd, A. D. 1985 Waves due to a steadily moving source on a floating ice plate. *J. Fluid Mech.* **158**, 269–287.

Garrett, C. & Munk, W. 1979 Internal waves in the ocean. *Ann. Rev. Fluid Mech.* **11**, 339–369.

Greenhill, A. G. 1887 Wavemotion in hydrodynamics. *Am. J. Math.* **9**, 62.

Kerr, A. D. 1979 The critical velocities of a floating ice plate subjected to in-plane forces and a moving load. *U.S. Army CRREL Res. Rep.* 79–19.

Kerr, A. D. 1983 The critical velocities of a moving load on a floating ice plate that is subjected to inplane forces. *Cold Regions Sci. Tech.* **6**, 267–274.

LAMB, H. 1945 *Hydrodynamics*. Dover.

LANDAU, L. D. & LIFSHITZ, E. M. 1959 *Theory of Elasticity*. Pergamon.

LEWIS, E. L. & WALKER, E. R. 1970 The water structure under a growing ice sheet. *J. Geophys. Res.* **75**, 6836–6845.

LIGHTHILL, M. J. 1978 *Waves in Fluids*. Cambridge University Press.

LONGUET-HIGGINS, M. S. 1977 Some effects of finite steepness on the generation of waves by wind. In *A Voyage of Discovery: George Deacon 70th Anniversary Volume* (ed. M. Angel), pp. 393–403, Pergamon

SEIFERT, W. F. & LANGLEBEN, M. P. 1972 Air drag coefficient and roughness length of a cover of sea ice. *J. Geophys. Res.* **77**, 2708–2713.

SQUIRE, V. A., ROBINSON, W. H., HASKELL, T. G. & MOORE, S. G. 1985 Dynamic strain response of lake and sea ice to moving loads. *Cold Regions Sci. Tech.*, **11**, 123–139.